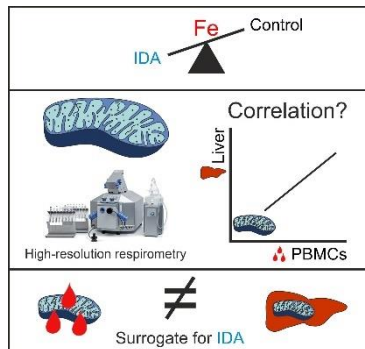


## Experimental Communication

### Cite

Fischer C, Valente de Souza L, Komlódi T, Garcia-Souza L, Volani C, Tymoszuk P, Demetz E, Seifert M, Auer K, Hilbe R, Brigo N, Petzer V, Asshoff M, Gnaiger E, Weiss G (2022) Mitochondrial respiration in response to iron deficiency anemia. Comparison of peripheral blood mononuclear cells and liver. MitoFit Preprints 2022.02.  
doi:10.26124/mitofit:2022-0002



Received 2022-03-01









Accepted 2022-03-02

Online 2022-03-04

### Author contributions

Conceptualization, CF and GW; methodology, CF, LVS, TK, LGS, CV, PT, EG, MS, KA, RH, NB, VP, MA, EG and GW; validation CF, LVS, TK, LGS, CV, PT, EG, MS, KA, RH, NB, VP, MA, EG and GW; formal analysis, CF and GW; resources, GW; writing—original draft preparation, CF and GW; writing—review and editing, CF, LVS, TK, LGS, CV, PT, EG, MS, KA, RH, NB, VP, MA, EG and GW; supervision, GW; funding acquisition, GW. All authors have read and agreed to the published version of the manuscript.

# Mitochondrial respiration in response to iron deficiency anemia. Comparison of peripheral blood mononuclear cells and liver

 Christine Fischer<sup>1</sup>, Lara Valente de Souza<sup>1</sup>,  Timea Komlódi<sup>2</sup>,  Luiz F Garcia-Souza<sup>2</sup>,  Chiara Volani<sup>1</sup>,  Piotr Tymoszuk<sup>1</sup>,  Egon Demetz<sup>1</sup>, Markus Seifert<sup>1,3</sup>, Kristina Auer<sup>1</sup>, Richard Hilbe<sup>1</sup>, Natascha Brigo<sup>1</sup>, Verena Petzer<sup>1</sup>, Malte Asshoff<sup>1</sup>,  Erich Gnaiger<sup>2</sup>,  Guenter Weiss<sup>1\*</sup>

<sup>1</sup> Dept Internal Medicine II, Medical Univ Innsbruck, Anichstrasse 35, 6020 Innsbruck, Austria

<sup>2</sup> Oroboros Instruments, Innsbruck, Austria

<sup>3</sup> Christian Doppler Laboratory for Iron Metabolism and Anemia Research, Medical Univ Innsbruck, Austria

\* Corresponding author: [guenter.weiss@i-med.ac.at](mailto:guenter.weiss@i-med.ac.at)

## Abstract

Iron is an essential component for metabolic processes including oxygen transport within hemoglobin, tricarboxylic acid (TCA) cycle activity and mitochondrial energy transformation. Iron deficiency can thus lead to metabolic dysfunction and eventually result in iron deficiency anemia (IDA) which affects approximately 1.5 billion people worldwide. Using a rat model of IDA induced by phlebotomy, we studied the effects of IDA on mitochondrial respiration in peripheral blood mononuclear cells (PBMCs) and liver. Furthermore, we evaluated whether mitochondrial function evaluated by high-resolution respirometry in PBMCs reflects corresponding alterations in the liver. Surprisingly, mitochondrial respiratory capacity was increased in PBMCs from rats with IDA compared to controls. In contrast, mitochondrial respiration remained unaffected in livers from IDA rats. Of note, citrate synthase activity indicated an increased mitochondrial density in

**Conflicts of interest**

The authors declare no conflict of interest.

**Keywords**

Anemia, iron deficiency, peripheral blood mononuclear cells, liver, mitochondrial function, OXPHOS, mitochondrial respiration, surrogate

**PBMCs, whereas it remained unchanged in the liver, partly explaining the different responses of mitochondrial respiration in PBMCs and liver. Taken together, these results indicate that mitochondrial function determined in PBMCs cannot serve as a valid surrogate for respiration in the liver. Metabolic adaptations to iron deficiency resulted in different metabolic reprogramming in the blood cells and liver tissue.**

## 1. Introduction

Anemia is a global burden affecting more than 1.5 billion people worldwide [1-3]. The most prevalent form of anemia is iron deficiency anemia (IDA), mostly occurring in preschool children and women in reproductive age [1,2]. The main symptoms include fatigue, weakness, and pale skin along with reduced cardio-vascular performance. Moreover, IDA may negatively affect growth and cognitive development of children [1,4,5]. IDA is characterized by absolute iron deficiency caused by chronic blood loss, insufficient dietary intake, or a combination of both [1,5].

Iron is an essential trace element for life, as it is necessary for hemoglobin biosynthesis and for key metabolic enzymes involved in DNA replication, hormone synthesis and mitochondrial bioenergetics [6,7]. Especially in mitochondria, iron is needed for heme synthesis, iron sulfur (Fe-S) cluster formation and oxidative phosphorylation [8-13]. In the electron transfer system (ETS) complexes CI, CII and CIII possess Fe-S clusters which are crucial for the synthesis of adenosine triphosphate (ATP). Iron metabolism is tightly regulated by the liver-derived peptide hormone hepcidin, which mediates degradation of ferroportin, the only cellular iron exporter known so far, thereby controlling iron absorption and iron recycling from macrophages [14]. Expression of hepcidin is controlled by multiple factors. Both iron deficiency and anemia reduce hepcidin expression, therefore increasing circulating iron levels and delivery to erythroid progenitor cells [3,14].

It has been shown previously that systemic iron deficiency and IDA reduce mitochondrial respiratory capacity in cardiomyocytes and skeletal muscle via reduction of iron-rich mitochondrial electron transfer components and morphologic changes of mitochondria such as reduced cristae structure [15-19]. In addition, mitochondria in hepatocytes of iron deficient rats exhibit ultrastructural abnormalities including an enlarged and rounded shape, therefore occupying an increased proportion of the cytoplasm due to their larger size but not due to an increased number of mitochondria [20,21].

Despite of possible implications of these morphologic alterations on mitochondrial function, the impact of IDA on mitochondrial respiration in circulating peripheral blood mononuclear cells (PBMCs) and liver has not been analyzed thus far. We studied these two systems since determination of mitochondrial function in PBMCs might represent an easily accessible surrogate reflecting mitochondrial functionality in the organs such as

the liver. Changes in mitochondrial respiration of PBMCs have been observed in various diseases including fatty liver disease, depression, or sepsis, and even in restless legs syndrome where impaired mitochondrial function was linked to indication of mitochondrial iron deficiency [22-25]. Therefore, analysis of PBMCs could be an efficient and minimal invasive procedure when relating information from blood samples to organ function or disease state instead of collecting biopsies from the particular organ itself.

The aim of this study was a comparative analysis of mitochondrial respiration in PBMCs and liver under steady-state control conditions and in the course of IDA.

## 2. Results

### 2.1. Effects of IDA on hematological and iron parameters

IDA was induced by phlebotomy for five consecutive days as previously described [26]. As anticipated, hemoglobin concentration was significantly lower in rats with IDA compared to controls (Figure 1a). Moreover, the reticulocyte fraction was increased (Figure 1b). Plasma iron concentration did not differ significantly (Figure 1c). The lymphocyte fraction remained unaffected (Figure 1d), whereas an increased proportion of monocytes altered PBMC composition in rats with IDA (Figure 1e). Hepatic mRNA expression (*Hamp*) of the master regulator of iron metabolism, hepcidin, was decreased (Figure 1f). Along with that, liver iron content was lower in IDA animals compared to controls (Figure 1g).

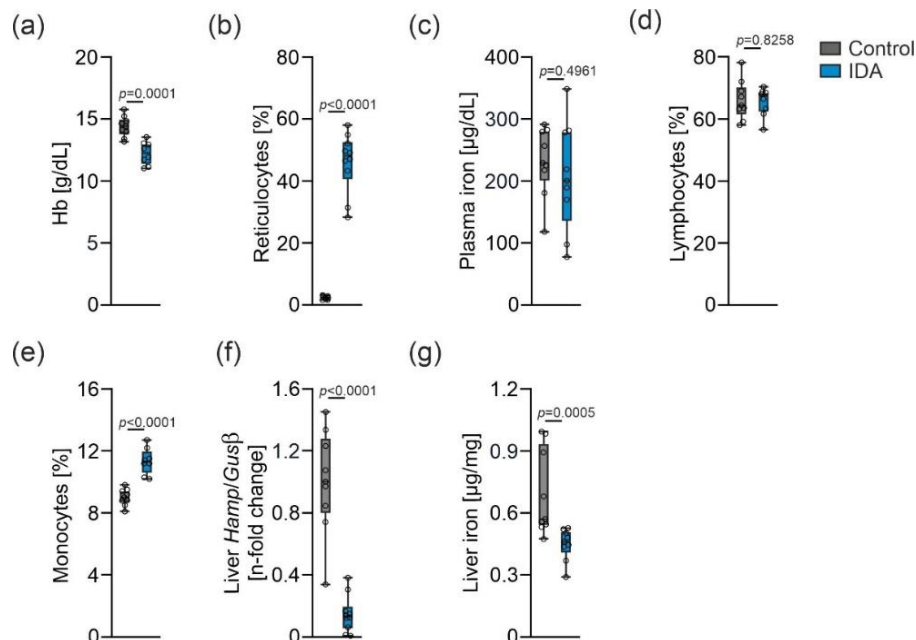


**Figure 1.** Alterations in blood and iron parameters caused by iron deficiency anemia (IDA).

(a) Hemoglobin (Hb) concentration; (b) reticulocyte proportion; (c) plasma iron concentration; (d) lymphocyte fraction; (e) monocyte fraction; (f) liver *Hamp*

mRNA expression relative to *glucuronidase beta* (*Gusβ*); and (g) liver iron content. Control  $N = 9$  rats, IDA  $N = 10$  rats. An unpaired two-tailed student's t-test was applied for all normal distributed results; a Mann-Whitney-U test was applied for the non-parametric result shown in (g). Values are shown as median  $\pm$  interquartile range.  $p$ -values are shown in the graphs.

## 2.2. Mitochondrial respiration differs in PBMCs and livers in response to IDA

We then analyzed the effects of IDA on mitochondrial respiratory capacity in freshly isolated PBMCs and homogenate from fresh liver biopsies (for protocols see Supplemental Figures S1 and S2). Of note, we observed an increase of mitochondrial respiration in PBMCs of IDA compared to control rats (Figure 2a). This included LEAK respiration (Figure 2a,  $PM_L$ ), OXPHOS capacity (Figure 2a,  $PM_P$ ) and electron transfer (ET) capacity (Figure 2a,  $PM_E$ ;  $PGMS_E$  and  $S_E$ ). In contrast, no major changes in liver mitochondrial respiratory capacity were observed when comparing IDA and control rats (Figure 2b).

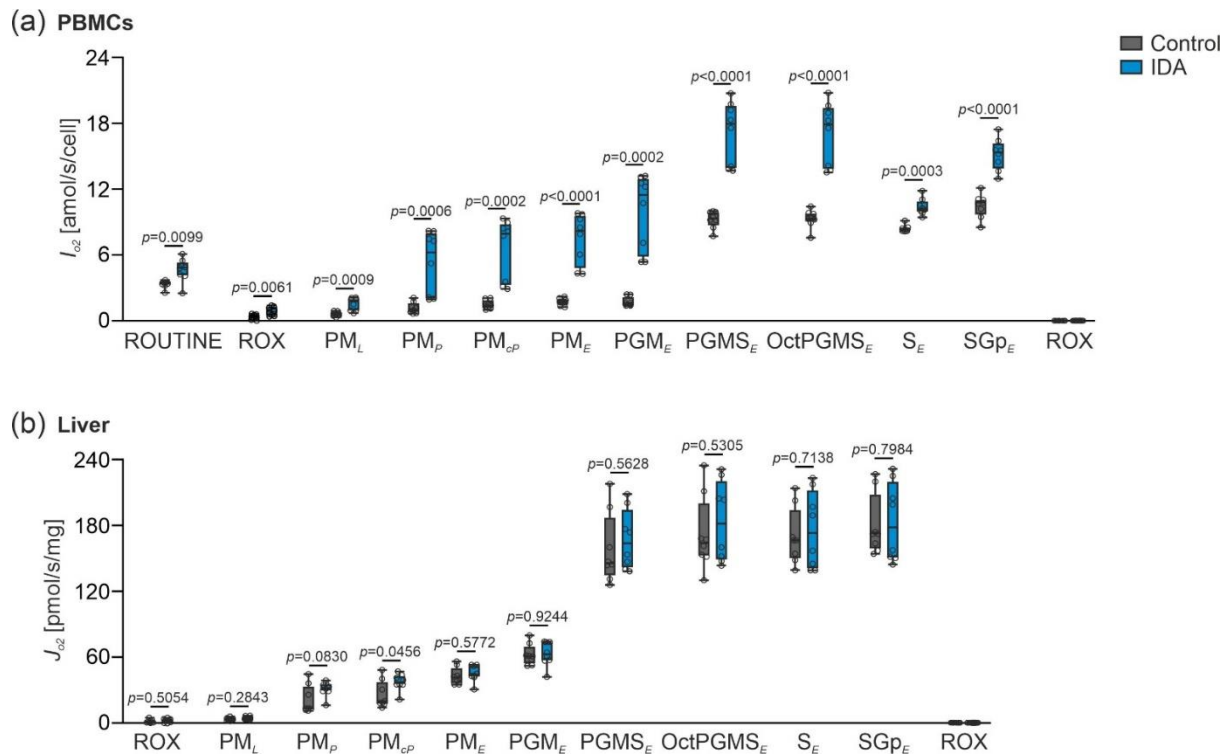


**Figure 2. Effects of IDA on mitochondrial respiration in rat peripheral blood mononuclear cells (PBMCs) and liver. (a)** Mitochondrial respiratory capacity in PBMCs with sequential titrations; states: ROUTINE: living cells, residual oxygen consumption (ROX): digitonin,  $PM_L$ : pyruvate + malate,  $PM_P$ : ADP,  $PM_{cP}$ : cytochrome c,  $PM_E$ : uncoupler carbonyl cyanide m-chloro phenyl hydrazine (CCCP),  $PGM_E$ : glutamate,  $PGMS_E$ : succinate, Oct $PGMS_E$ : octanoylcarnitine,  $S_E$ : rotenone,  $SGp_E$ : glycerophosphate, ROX: antimycin A. **(b)** Mitochondrial respiratory capacity in the liver; states: ROX: liver homogenate,  $PM_L$ : pyruvate + malate,  $PM_P$ : ADP,  $PM_{cP}$ : cytochrome c,  $PM_E$ : uncoupler CCCP,  $PGM_E$ : glutamate,  $PGMS_E$ : succinate, Oct $PGMS_E$ : octanoylcarnitine,  $S_E$ : rotenone,  $SGp_E$ : glycerophosphate, ROX: antimycin A.  $N = 8$  rats per group. An unpaired two-tailed student's t-test was applied for all normal distributed states; a Mann-Whitney-U test was applied for the non-parametric states **(a)**  $PM_P$ ,  $PM_{cP}$ ,  $PGM_E$ ,  $S_E$ ; **(b)** ROX,  $PM_P$ ,  $SGp_E$ . Values are shown as median  $\pm$  interquartile range.  $p$ -Values are shown in the graphs.

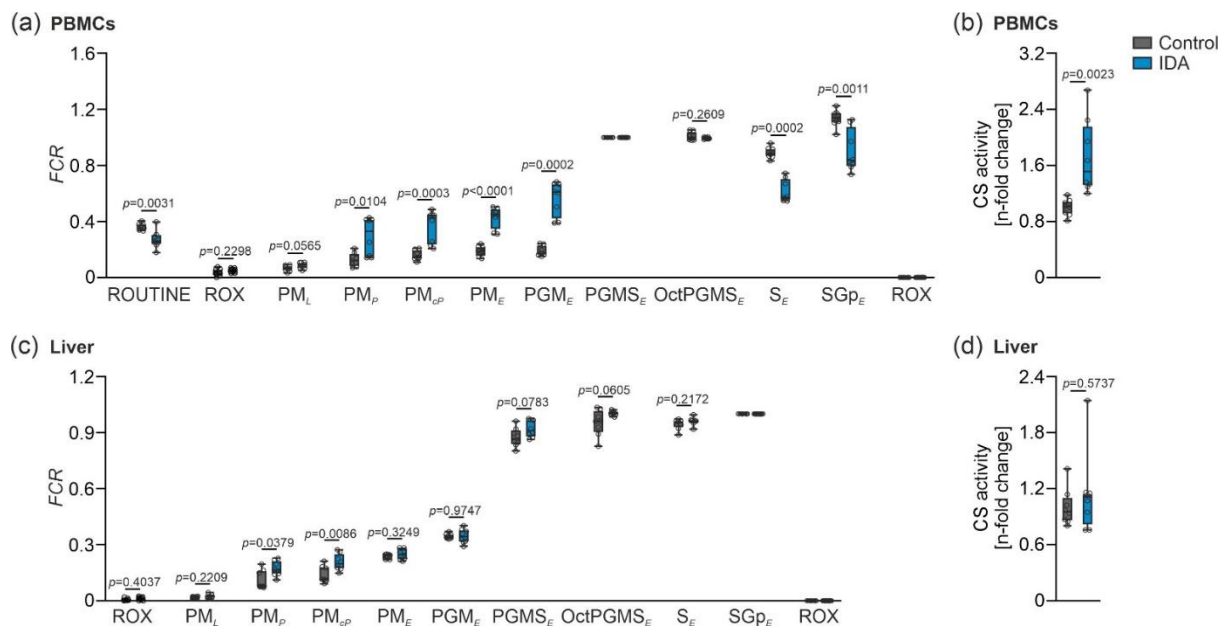


**Figure 3. Mitochondrial respiration in PBMCs and liver from control and IDA rats independent of mitochondrial density and citrate synthase (CS) activity. (a)** *FCR* calculated from PBMC respiration with reference state PGMS<sub>E</sub>. States: ROUTINE: living cells, ROX: digitonin, PM<sub>L</sub>: pyruvate + malate, PM<sub>P</sub>: ADP, PM<sub>CP</sub>: cytochrome c, PM<sub>E</sub>: uncoupler CCCP, PGM<sub>E</sub>: glutamate, PGMS<sub>E</sub>: succinate, OctPGMS<sub>E</sub>: octanoylcarnitine, S<sub>E</sub>: rotenone, SGp<sub>E</sub>: glycerophosphate, ROX: antimycin A. **(c)** *FCR* calculated from liver respiration with reference state SGp<sub>E</sub>. States: ROX: liver homogenate, PM<sub>L</sub>: pyruvate + malate, PM<sub>P</sub>: ADP, PM<sub>CP</sub>: cytochrome c, PM<sub>E</sub>: uncoupler CCCP, PGM<sub>E</sub>: glutamate, PGMS<sub>E</sub>: succinate, OctPGMS<sub>E</sub>: octanoylcarnitine, S<sub>E</sub>: rotenone, SGp<sub>E</sub>: glycerophosphate, ROX: antimycin A. **(b)** and **(d)** CS activity in PBMCs and liver, respectively. Values of CS activity are shown as n-fold change of control. *N* = 8 rats per group. An unpaired two-tailed student's t-test was applied for all normal distributed results; a Mann-Whitney-U test was applied for the non-parametric results **(a)** PM<sub>P</sub>, PM<sub>CP</sub>, PGM<sub>E</sub>, S<sub>E</sub>; **(b)** PM<sub>P</sub> and **(d)**. Values are shown as median ± interquartile range. *p*-Values are shown in the graphs.

We next investigated whether tissue specific alterations of mitochondrial function could be based on changes in mitochondrial quality and density in response to IDA. Therefore, flux control ratios (*FCR*) were calculated in both, PBMCs and liver, whereby the values obtained from the measurements of mitochondrial respiration were normalized for a common reference state (PBMCs: PGMS<sub>E</sub>; liver: SGp<sub>E</sub>) showing mitochondrial respiration independent of mitochondrial density (Figure 3a and c) [13,27,28]. In PBMCs, increased mitochondrial respiration was still observed after correction for mitochondrial density in OXPHOS (Figure 3a, state PM<sub>P</sub>) and ET (Figure 3a, state PM<sub>E</sub> and S<sub>E</sub>). Furthermore, citrate synthase (CS) activity, a marker for mitochondrial density, was measured [29-31]. In PBMCs, CS activity was significantly increased (Figure 3b). Consequently, the observed changes in mitochondrial respiration in PBMCs originated from alterations in mitochondrial quality and mitochondrial density. In the liver, we found a slight increase in OXPHOS capacity whereas all other measurements of

mitochondrial function remained unaffected when comparing control to IDA animals (Figure 3c, state  $PM_P$ ). CS activity in the liver did not show any differences (Figure 3d), indicating that mitochondrial density remained unaltered when comparing IDA with control rats, and supporting the conclusion of unchanged mitochondrial quality drawn from the *FCR*.

Having observed tissue-specific differences in mitochondrial function in PBMCs compared to the liver of control and IDA animals, we next studied for the possibility of mitochondrial damage. As a surrogate we investigated a potential loss of mitochondrial outer membrane mtOM integrity by quantifying the cytochrome *c* control efficiency  $j_{cyt\ c}$  [11].  $j_{cyt\ c}$  did not show significant differences neither in PBMCs nor in the liver when comparing control to IDA rats (Figure 4a and b). Consequently, damage of the mtOM could be ruled out as a cause for differences in PBMC mitochondrial respiration between the two groups. Furthermore, in PBMCs of IDA rats an increase in *E-L* coupling efficiency was detected (Figure 4c), indicating an improved coupling of the ET to the phosphorylation of ADP. This may likewise be underlying the observed increase in mitochondrial respiration. In the liver, *E-L* coupling efficiency remained stable (Figure 4d), whereas the *E-P* control efficiency was decreased in IDA liver homogenates as compared to the controls (Figure 4f), indicating a decreased capacity of the oxidative phosphorylation system [13,28,32]. In PBMCs, the *E-P* control efficiency remained unchanged (Figure 4e).

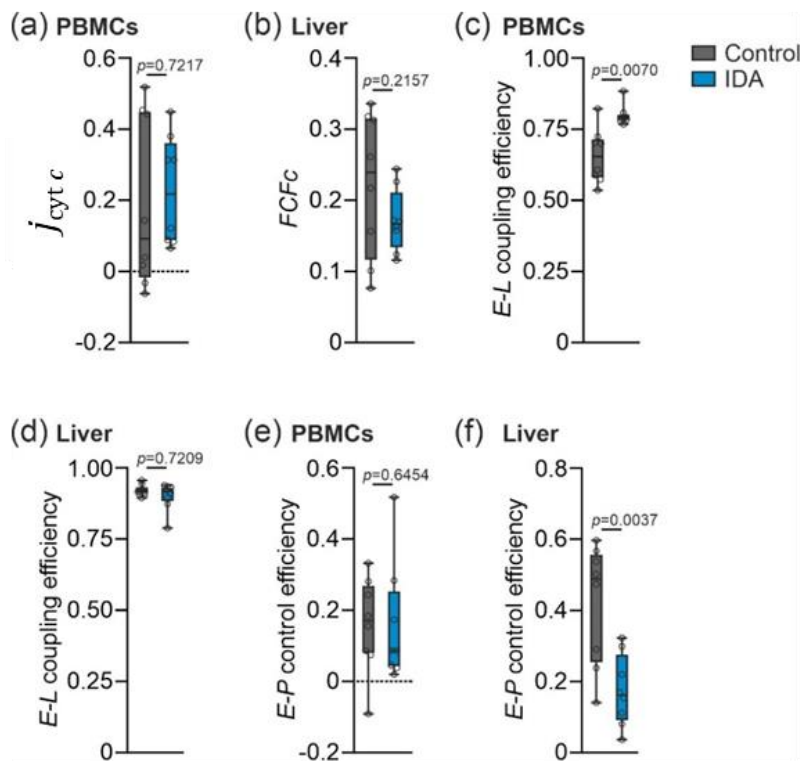


**Figure 4. Effects of IDA on flux control efficiencies in rat PBMCs and liver. (a) and (b) Cytochrome *c* control efficiency ( $j_{cyt\ c} = 1 - PM_P/PM_{cP}$ ) indicates integrity of the outer mitochondrial membrane. (c) and (d) *E-L* coupling efficiency ( $j_{E-L} = 1 - PM_L/PM_E$ ) indicates preserved coupling of electron transfer to phosphorylation of ADP. (e) and (f) *E-P* control efficiency ( $1 - PM_{cP}/PM_E$ ) indicates the limitation of the OXPHOS capacity due to the capacity of the phosphorylation system.  $N = 8$  rats per group. An**

unpaired two-tailed student's t-test was applied for all normal distributed results; a Mann-Whitney-U test was applied for the non-parametric results shown in (c), (d) and (e). Values are shown as median  $\pm$  interquartile range. *p*-Values are shown in the graphs.

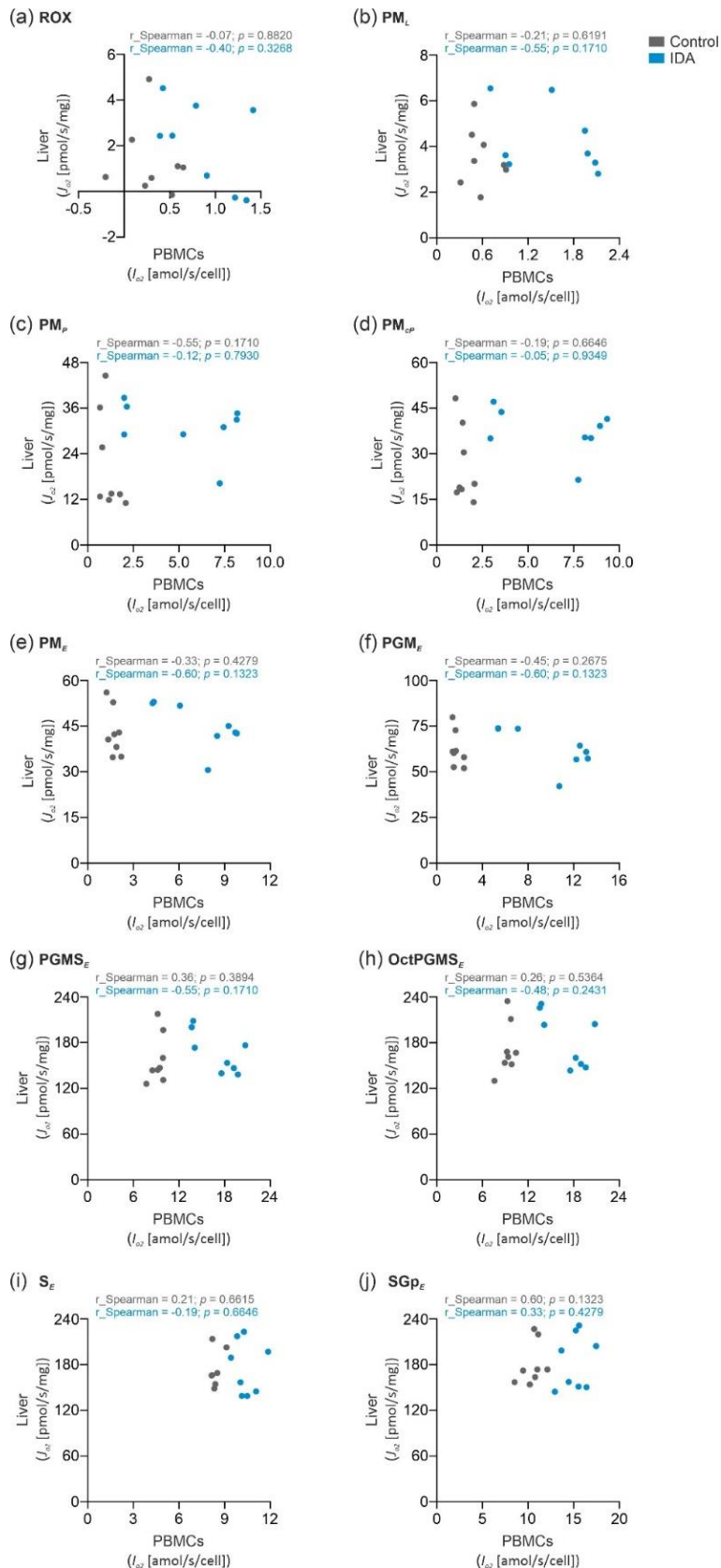


**Figure 5. Correlation analysis of PBMC mitochondrial respiration and liver mitochondrial respiration in control and IDA.** Spearman's rank correlation in the measured respiratory states in PBMCs and liver: **(a)** ROX; **(b)**  $\text{PM}_L$ ; **(c)**  $\text{PM}_p$ ; **(d)**  $\text{PM}_{cp}$ ; **(e)**  $\text{Pm}_E$ ; **(f)**  $\text{PGM}_p$ ; **(g)**  $\text{PGMSE}$ ; **(h)** Oct $\text{PGMSE}$ ; **(i)**  $\text{SE}$ ; **(j)**  $\text{SGp}_E$ .  $N = 8$  rats per group. Statistical significance of the correlation was tested using an unpaired two-tailed student's t-test. The correlation coefficients ( $r_{\text{Spearman}}$ ) and the  $p$ -values are shown in the graphs.

### 2.3. PBMC mitochondrial respiration was not correlated with liver mitochondrial respiration

To investigate if mitochondrial respiration in PBMCs reflects liver mitochondrial respiration, we analyzed the correlation of the respiratory states shown in section 2.2. (Figure 5a-j). In none of the states, PBMC mitochondrial respiration was significantly linked to liver mitochondrial respiration. Consequently, measurement of mitochondrial respiration in PBMCs does not reflect liver mitochondrial function. Nevertheless, PBMCs may be used as a surrogate for mitochondrial dysfunction in other specific diseases.

### 3. Discussion

We found that IDA led to different effects on mitochondrial respiratory capacity in permeabilized PBMCs and liver homogenates. Surprisingly, IDA resulted in an increase of mitochondrial activity in PBMCs for which different factors may be responsible. We observed a relative expansion of monocytes when comparing PBMCs from IDA versus control animals. Thus, it will be of interest in future investigations to study if mitochondrial respiratory capacity differs between various leucocyte species in general, but also in response to iron deficiency as suggested in previous studies [33,34]. However, in contrast to these studies, we did not detect any differences in mitochondrial outer membrane integrity as determined by the  $j_{\text{cyt } c}$ , but we found an increase in mitochondrial density in PBMCs as shown by higher CS activity, likewise explaining the increase in mitochondrial respiration. Nonetheless, the increase in mitochondrial activity in PBMCs of IDA rats was surprising because iron deficiency *in vitro* has been demonstrated to result in impaired Fe-S cluster synthesis for the respiratory complexes and reduced mitochondrial activity [8,9,35]. However, most of those studies have been performed *in vitro* and iron deficiency was often induced by the addition of an iron chelator. Nonetheless, the increase in mitochondrial density suggests the presence of a compensatory mechanism, by which mitochondrial number or longevity of mitochondria increase to compensate for impaired mitochondrial activity as a consequence of iron deficiency. This is in line with a recent observation indicating that the age of mitochondria determines their metabolic activity [36].

Compared to the results of mitochondrial activity in cardiomyocytes and skeletal muscle fibers described in literature, mitochondria in the liver did not show a decrease in mitochondrial respiration induced by IDA in our study [15-19]. Plausible explanations might be that those studies on morphological changes of mitochondria in different organs and cells used mostly animals whose iron deficiency or IDA was induced over a longer period of time [15-21]. In contrast, we used a short-term phlebotomy model to induce IDA that might not reduce the amount of iron in the liver to an extent required for restricting iron supply to mitochondria leading to impairment of mitochondrial respiration. In addition, the liver is a central organ of iron storage and iron regulation. Therefore, short-term induction of iron deficiency by phlebotomy may be compensated by iron mobilization within this organ, thereby delivering enough iron to maintain hepatic mitochondrial function. It will be of interest to study, if long-lasting persistence of iron deficiency changes the phenotype of hepatic mitochondrial function. This is indicated by observations made in mice with genetic and dietary iron overload, where only long-term exposure to those stressors resulted in altered mitochondrial iron status and activity [13]. Finally, it has to be kept in mind that iron availability affects multiple other metabolic pathways including tricarboxylic acid (TCA) cycle activity, lipid and protein synthesis, which may affect mitochondrial structure and function [37].

Our study suggests that mitochondrial function in PBMCs and liver is not comparable at least in the setting of IDA. Therefore, changes in mitochondrial activity in PBMCs are not associated with alterations of mitochondrial function in the liver. Our results do not exclude, however, that mitochondrial activity in PBMCs may indicate



principal defects or alterations of mitochondrial function present in other specific diseases.

## 4. Materials and methods

### 4.1. Animal experiments

All rat experiments were performed as described before [26]. Age-matched female Lewis rats (Charles River Laboratories, United Kingdom) were kept on a standard rodent diet containing 180 mg Fe/kg (Ssniff, Soest, Germany) until they reached an age of 8 to 11 weeks. The animals had free access to food and water and were kept according to institutional and governmental guidelines in the animal housing unit of the Medical University of Innsbruck with a 12 h light-dark cycle and an average temperature of 20 °C ± 1 °C. All animal experiments were approved by the Austrian Federal Ministry of Science and Research (BMWFV-66.011/0138-WF/V/3b/2016).

Half of the rats were phlebotomized, 1.8 mL blood was sampled daily for five consecutive days (starting one week before death) to induce IDA. After termination of the experiment, organs and blood were harvested for further analysis. Total blood counts were measured using a VetABC animal blood counter (Scil Animal Care, Viernheim, Germany).

### 4.2. Reticulocyte quantification

Peripheral reticulocytes were measured using flow cytometry. Briefly, full blood was stained with Thiazole Orange (Santa Cruz, Dallas, TX, USA) and after identification of the single cells using forward and side scatters, the Thiazole Orange positive cells were identified as reticulocytes.

### 4.3. Isolation of PBMCs

PBMCs were isolated as described before [22]. Briefly, rat full blood was diluted 1:3 with phosphate buffered saline (PBS, Lonza Bioscience, Basel, Switzerland) and loaded onto Pancoll separating solution (density 1.077 g/mL, PAN-Biotech, Aidenbach, Germany). After centrifugation (1,000 g, 10 min, no brake) the buffy coat was collected, and the cells were washed twice with PBS.

### 4.4. High-resolution respirometry

All measurements were performed as described before [13,27,28]. Briefly, mitochondrial respiration was performed using the Oxygraph-2k (O2k, Oroboros Instruments, Innsbruck, Austria). Fresh rat liver tissue samples were collected and homogenized and PBMCs were isolated from blood samples. Respiratory measurements of isolated PBMCs ( $2 \times 10^6$  cells/mL) and liver tissue homogenate (0.5 mg/mL) were performed at kinetically saturating oxygen concentrations in mitochondrial respiration medium MiR05-Kit (Oroboros Instruments) containing 0.5 mM ethylene glycol tetraacetic acid (EGTA), 3 mM magnesium chloride ( $\text{MgCl}_2$ ), 60 mM lactobionic acid, 20 mM taurine, 10 mM monopotassium phosphate ( $\text{KH}_2\text{PO}_4$ ), 20 mM 4-(2-hydroxyethyl)-1-

piperazineethanesulfonic acid (HEPES), 110 mM D-sucrose supplemented with 1 g/l essentially fatty acid-free bovine serum albumin (BSA, Sigma-Aldrich, St. Louis, MO, USA). Manual titrations of substrates, uncoupler, and inhibitors were performed using Hamilton syringes (customized for Oroboros Instruments, Hamilton Central Europe, Giarmata, Romania). The following substrate-uncoupler-inhibitor titration (SUIT) protocol was used (Supplemental Figures S1 and S2) [38,39]: Isolated PBMCs were permeabilized using digitonin (Dig, 2  $\mu\text{g}/\text{mL}$ ): ROX; non-phosphorylating LEAK respiration was assessed by injecting pyruvate (P, 5 mM) and malate (M, 2 mM) as NADH (N)-linked substrates in the absence of adenylates:  $\text{PM}_L$ ; OXPHOS capacity was measured by adding adenosine diphosphate (ADP, 2.5 mM) at kinetically saturating concentration:  $\text{PM}_P$ ; cytochrome c (c, 10  $\mu\text{M}$ ) was added to test for the mitochondrial outer membrane integrity:  $\text{PM}_{cP}$ ; stepwise titrations of the protonophore carbonyl cyanide m-chloro phenyl hydrazine (U, 0.5  $\mu\text{M}$  steps) allowed to reach the maximal electron transfer (ET) capacity:  $\text{PM}_E$ ; glutamate (10 mM) was added as an N-linked substrate in non-coupled ET state:  $\text{PGM}_E$ ; by addition of succinate (S, 10 mM) the simultaneous action of N-linked substrates and succinate with convergent electron flow in the NS-pathway for reconstitution of the TCA cycle function was measured:  $\text{PGMS}_E$ ; titration of octanoylcarnitine (Oct, 0.5 mM) enabled the simultaneous action of F-and N-linked substrates and S with convergent electron flow in the FNS pathway for reconstitution of TCA cycle function and additive or inhibitory effect of F-linked substrate Oct to support fatty acid oxidation:  $\text{OctPGMS}_E$ ; CI inhibition by rotenone (Rot, 0.5  $\mu\text{M}$ ) induced succinate-linked ET capacity:  $S_E$ ; titration of glycerophosphate (Gp, 10 mM) provided simultaneous action of convergent S-and Gp-linked electron entry in the SGp-pathway:  $\text{SGp}_E$ ; injection of antimycin A (2.5  $\mu\text{M}$ ) blocked CIII and induced the state of residual oxygen consumption: ROX. Data analysis was performed using the software DatLab 7.4 (Oroboros Instruments).

#### 4.5. Plasma and total tissue iron

Plasma iron was measured using QuantiChrom Iron Assay kit (BioAssay Systems, Hayward, CA, USA) according to the manufacturer's instructions. Tissue iron determination was performed as described [13,28,40]. After acidic hydrolysis at 65 °C for 24 h, the iron content was measured using a colorimetric staining solution containing sodium acetate and bathophenanthroline disulfonic acid. Total tissue iron content was normalized by protein content.

#### 4.6. RNA extraction and quantitative real-time PCR

Liver total RNA was extracted using TRI reagent (Sigma-Aldrich) according to the manufacturer's protocol. After reverse transcription, mRNA expression was analyzed as described [13,41]. The following primers were used: *Hamp* forward 5'-TGAGCAGCGGTGCCTATCT-3', *Hamp* reverse 5'-CCATGCCAAGGCTGCAG-3', *Hamp* probe FAM-CGGCAACAGACGAGACAGACTACGGC-BHQ1, *Gus $\beta$*  forward 5'-ATTACTCGAACAATCGGTTGCA-3', *Gus $\beta$*  reverse 5'-GACCGGCATGTCCAAGGTT-3', *Gus $\beta$*  probe FAM-CGTAGCGGCTGCCGGTACCACT-BHQ1. Quantitative real-time PCR reactions were performed on the CFX96 PCR System (BioRad, Hercules, CA, USA). Relative gene

expression was calculated with the  $\Delta\Delta C_t$  method in the CFX96 Manager software (BioRad). The housekeeping gene *Gus $\beta$*  was used as reference control.

#### 4.7. CS activity

CS activity was measured as described [13,28]. A spectrophotometric assay was used to measure the enzyme activity in snap-frozen liver homogenates. The sample enzymatic reaction mix contained 0.25 % Triton X-100 in aqua dest, 0.31 mM acetyl-coenzyme A in aqua dest, 0.1 mM 5,50-dithiobis-(2-nitrobenzoic acid) in 1 M Tris-HCl buffer (pH 8.1) and 0.5 mM oxaloacetate in 0.1M triethanolamine-HCl-buffer (pH 8.0). The absorbance of the reaction product thionitrobenzoic acid was measured at 412 nm over 200 s. The resulting enzyme activities were normalized by the protein content of the samples.

#### 4.8. Statistics

Statistical analysis was carried out using the software GraphPad Prism 9. In case of normal distribution statistical significance was determined by an unpaired two-tailed student's t-test. Otherwise, a Mann-Whitney U test was applied. To assess whether PBMC mitochondrial respiration is correlated to liver mitochondrial respiration, a Spearman's rank correlation analysis with a two-tailed student's test was performed. Data was shown as median  $\pm$  interquartile range. *p*-Values below 0.05 were considered significant.

#### Funding

This research was funded by the Christian Doppler Laboratory for Iron Metabolism and Anemia Research, the FWF funded doctoral program HOROS (W-1253, to GW) and the transnational doctoral program BI-DOC between the Medical University of Innsbruck, Austria and the Institute of Biomedicine, Eurac, in Bolzano, Italy.

#### Institutional Review Board Statement

The animal experiments in this study were approved by the Austrian Federal Ministry of Science and Research (BMWFV-66.011/0138-WF/V/3b/2016).

#### References

1. Camaschella, C. Iron-Deficiency Anemia. *New England Journal of Medicine* **2015**, *372*, 1832-1843, doi:10.1056/NEJMra1401038.
2. Kassebaum, N. J. The Global Burden of Anemia. *Hematol Oncol Clin North Am* **2016**, *30*, 247-308, doi:10.1016/j.hoc.2015.11.002.
3. Lanser, L., Burkert, F. R., Bellmann-Weiler, R., Schroll, A., Wildner, S., Fritsche, G. and Weiss, G. Dynamics in Anemia Development and Dysregulation of Iron Homeostasis in Hospitalized Patients with COVID-19. *Metabolites* **2021**, *11*, 653.
4. Sachdev, H. P. S., Gera, T. and Nestel, P. Effect of iron supplementation on mental and motor development in children: systematic review of randomised controlled trials. *Public Health Nutrition* **2005**, *8*, 117-132, doi:10.1079/PHN2004677.
5. Pasricha, S.-R., Tye-Din, J., Muckenthaler, M. U. and Swinkels, D. W. Iron deficiency. *The Lancet* **2021**, *397*, 233-248, doi:https://doi.org/10.1016/S0140-6736(20)32594-0.

6. Muckenthaler, M. U., Rivella, S., Hentze, M. W. and Galy, B. A Red Carpet for Iron Metabolism. *Cell* **2017**, *168*, 344-361, doi:10.1016/j.cell.2016.12.034.
7. Katsarou, A. and Pantopoulos, K. Basics and principles of cellular and systemic iron homeostasis. *Mol Aspects Med* **2020**, *75*, 100866, doi:10.1016/j.mam.2020.100866.
8. Lill, R. Function and biogenesis of iron-sulphur proteins. *Nature* **2009**, *460*, 831-838, doi:10.1038/nature08301.
9. Oexle, H., Gnaiger, E. and Weiss, G. Iron-dependent changes in cellular energy metabolism: influence on citric acid cycle and oxidative phosphorylation. *Biochimica et Biophysica Acta (BBA) - Bioenergetics* **1999**, *1413*, 99-107, doi:https://doi.org/10.1016/S0005-2728(99)00088-2.
10. Wang, J. and Pantopoulos, K. Regulation of cellular iron metabolism. *Biochemical Journal* **2011**, *434*, 365-381, doi:10.1042/bj20101825.
11. Gnaiger, E. Mitochondrial pathways and respiratory control. An introduction to OXPHOS analysis. 5th ed. *Bioenergetics Communications* **2020**, *2020.2*, 112pp, doi:doi:10.26124/bec:2020-0002.
12. Gnaiger, E. et al. — MitoEAGLE Task Group. Mitochondrial physiology. *Bioenergetics Communications* **2020**, *2020.1*, doi:https://doi.org/10.26124/bec:2020-0001.v1
13. Fischer, C., Volani, C., Komlódi, T., Seifert, M., Demetz, E., Valente de Souza, L., Auer, K., Petzer, V., von Raffay, L., Moser, P.; et al. Dietary Iron Overload and Hfe-/- Related Hemochromatosis Alter Hepatic Mitochondrial Function. *Antioxidants* **2021**, *10*, 1818.
14. Nemeth, E. and Ganz, T. Hepcidin-Ferroportin Interaction Controls Systemic Iron Homeostasis. *International journal of molecular sciences* **2021**, *22*, 6493, doi:10.3390/ijms22126493.
15. Macdonald, V. W. and Jacobus, W. E. Substrate-dependent functional defects and altered mitochondrial respiratory capacity in hearts from guinea pigs with iron deficiency anemia. *Biochimica et Biophysica Acta (BBA) - Bioenergetics* **1987**, *891*, 103-114, doi:https://doi.org/10.1016/0005-2728(87)90001-6.
16. Hoes, M. F., Grote Beverborg, N., Kijlstra, J. D., Kuipers, J., Swinkels, D. W., Giepmans, B. N. G., Rodenburg, R. J., van Veldhuisen, D. J., de Boer, R. A. and van der Meer, P. Iron deficiency impairs contractility of human cardiomyocytes through decreased mitochondrial function. *Eur J Heart Fail* **2018**, *20*, 910-919, doi:10.1002/ehjhf.1154.
17. Cartier, L. J., Ohira, Y., Chen, M., Cuddihee, R. W. and Holloszy, J. O. Perturbation of mitochondrial composition in muscle by iron deficiency. Implications regarding regulation of mitochondrial assembly. *Journal of Biological Chemistry* **1986**, *261*, 13827-13832, doi:https://doi.org/10.1016/S0021-9258(18)67094-2.
18. Rineau, E., Gaillard, T., Gueguen, N., Procaccio, V., Henrion, D., Prunier, F. and Lasocki, S. Iron deficiency without anemia is responsible for decreased left ventricular function and reduced mitochondrial complex I activity in a mouse model. *Int J Cardiol* **2018**, *266*, 206-212, doi:10.1016/j.ijcard.2018.02.021.
19. McKay, R. H., Higuchi, D. A., Winder, W. W., Fell, R. D. and Brown, E. B. Tissue effects of iron deficiency in the rat. *Biochimica et Biophysica Acta (BBA) - General Subjects* **1983**, *757*, 352-358, doi:https://doi.org/10.1016/0304-4165(83)90061-2.
20. Dallman, P. R. and Goodman, J. R. Enlargement of Mitochondrial Compartment in Iron and Copper Deficiency. *Blood* **1970**, *35*, 496-505, doi:https://doi.org/10.1182/blood.V35.4.496.496.
21. Dallman, P. R. and Goodman, J. R. The effects of iron deficiency on the hepatocyte: a biochemical and ultrastructural study. *J Cell Biol* **1971**, *48*, 79-90, doi:10.1083/jcb.48.1.79.
22. Haschka, D., Volani, C., Stefani, A., Tymoszek, P., Mitterling, T., Holzknicht, E., Heidbreder, A., Coassin, S., Sumbalova, Z., Seifert, M.; et al. Association of mitochondrial iron deficiency and

- dysfunction with idiopathic restless legs syndrome. *Movement Disorders* **2019**, *34*, 114-123, doi:<https://doi.org/10.1002/mds.27482>.
23. Ajaz, S., McPhail, M. J., Gnudi, L., Trovato, F. M., Mujib, S., Napoli, S., Carey, I. and Agarwal, K. Mitochondrial dysfunction as a mechanistic biomarker in patients with non-alcoholic fatty liver disease (NAFLD). *Mitochondrion* **2021**, *57*, 119-130, doi:<https://doi.org/10.1016/j.mito.2020.12.010>.
  24. Belikova, I., Lukaszewicz, A. C., Faivre, V., Damoiseil, C., Singer, M. and Payen, D. Oxygen consumption of human peripheral blood mononuclear cells in severe human sepsis. *Crit Care Med* **2007**, *35*, 2702-2708, doi:10.1097/01.ccm.0000295593.25106.c4.
  25. Japiassú, A. M., Santiago, A. P., d'Avila, J. C., Garcia-Souza, L. F., Galina, A., Castro Faria-Neto, H. C., Bozza, F. A. and Oliveira, M. F. Bioenergetic failure of human peripheral blood monocytes in patients with septic shock is mediated by reduced F1Fo adenosine-5'-triphosphate synthase activity. *Crit Care Med* **2011**, *39*, 1056-1063, doi:10.1097/CCM.0b013e31820eda5c.
  26. Theurl, I., Aigner, E., Theurl, M., Nairz, M., Seifert, M., Schroll, A., Sonnweber, T., Eberwein, L., Witcher, D. R., Murphy, A. T.; et al. Regulation of iron homeostasis in anemia of chronic disease and iron deficiency anemia: diagnostic and therapeutic implications. *Blood* **2009**, *113*, 5277-5286, doi:10.1182/blood-2008-12-195651.
  27. Doerrier, C., Garcia-Souza, L. F., Krumschnabel, G., Wohlfarter, Y., Mészáros, A. T. and Gnaiger, E. High-Resolution FluoRespirometry and OXPHOS Protocols for Human Cells, Permeabilized Fibers from Small Biopsies of Muscle, and Isolated Mitochondria. In *Mitochondrial Bioenergetics: Methods and Protocols*, Palmeira, C.M., Moreno, A.J., Eds.; Springer New York: New York, NY, 2018; pp. 31-70.
  28. Volani, C., Doerrier, C., Demetz, E., Haschka, D., Paglia, G., Lavdas, A. A., Gnaiger, E. and Weiss, G. Dietary iron loading negatively affects liver mitochondrial function. *Metallomics* **2017**, *9*, 1634-1644, doi:10.1039/c7mt00177k.
  29. Holloszy, J. O., Oscai, L. B., Don, I. J. and Molé, P. A. Mitochondrial citric acid cycle and related enzymes: Adaptive response to exercise. *Biochemical and Biophysical Research Communications* **1970**, *40*, 1368-1373, doi:[https://doi.org/10.1016/0006-291X\(70\)90017-3](https://doi.org/10.1016/0006-291X(70)90017-3).
  30. Hood, D. A., Zak, R. and Pette, D. Chronic stimulation of rat skeletal muscle induces coordinate increases in mitochondrial and nuclear mRNAs of cytochrome-c-oxidase subunits. *Eur J Biochem* **1989**, *179*, 275-280, doi:10.1111/j.1432-1033.1989.tb14551.x.
  31. Williams, R. S., Salmons, S., Newsholme, E. A., Kaufman, R. E. and Mellor, J. Regulation of nuclear and mitochondrial gene expression by contractile activity in skeletal muscle. *J Biol Chem* **1986**, *261*, 376-380.
  32. Gnaiger, E., Boushel, R., Søndergaard, H., Munch-Andersen, T., Damsgaard, R., Hagen, C., Díez-Sánchez, C., Ara, I., Wright-Paradis, C., Schrauwen, P.; et al. Mitochondrial coupling and capacity of oxidative phosphorylation in skeletal muscle of Inuit and Caucasians in the arctic winter. *Scandinavian Journal of Medicine & Science in Sports* **2015**, *25*, 126-134, doi:<https://doi.org/10.1111/sms.12612>.
  33. Distante, S., Eikeland, J., Pawar, T., Skinnis, R., Høie, K., You, P., Mørkrid, L. and Eide, L. Blood removal therapy in hereditary hemochromatosis induces a stress response resulting in improved genome integrity. *Transfusion* **2016**, *56*, 1435-1441, doi:<https://doi.org/10.1111/trf.13588>.
  34. Jarvis, J. H. and Jacobs, A. Morphological abnormalities in lymphocyte mitochondria associated with iron-deficiency anaemia. *J Clin Pathol* **1974**, *27*, 973-979, doi:10.1136/jcp.27.12.973.
  35. Theurl, I., Schroll, A., Nairz, M., Seifert, M., Theurl, M., Sonnweber, T., Kulaksiz, H. and Weiss, G. Pathways for the regulation of hepcidin expression in anemia of chronic disease and iron

- deficiency anemia in vivo. *Haematologica* **2011**, *96*, 1761-1769, doi:10.3324/haematol.2011.048926.
36. Döhla, J., Kuuluvainen, E., Gebert, N., Amaral, A., Englund, J. I., Gopalakrishnan, S., Konovalova, S., Nieminen, A. I., Salminen, E. S., Torregrosa Muñumer, R.; et al. Metabolic determination of cell fate through selective inheritance of mitochondria. *Nat Cell Biol* **2022**, *24*, 148-154, doi:10.1038/s41556-021-00837-0.
  37. Volani, C., Paglia, G., Smarason, S. V., Pramstaller, P. P., Demetz, E., Pfeifhofer-Obermair, C. and Weiss, G. Metabolic Signature of Dietary Iron Overload in a Mouse Model. *Cells* **2018**, *7*, doi:10.3390/cells7120264.
  38. SUIT-001 O2 ce-pce D003. Available online: [https://www.bioblast.at/index.php/SUIT-001\\_O2\\_ce-pce\\_D003](https://www.bioblast.at/index.php/SUIT-001_O2_ce-pce_D003) (accessed on 23 February 2022).
  39. SUIT-001 O2 mt D001. Available online: [https://www.bioblast.at/index.php/SUIT-001\\_O2\\_mt\\_D001](https://www.bioblast.at/index.php/SUIT-001_O2_mt_D001) (accessed on 23 February 2022).
  40. Sonnweber, T., Ress, C., Nairz, M., Theurl, I., Schroll, A., Murphy, A. T., Wroblewski, V., Witcher, D. R., Moser, P., Ebenbichler, C. F.; et al. High-fat diet causes iron deficiency via hepcidin-independent reduction of duodenal iron absorption. *The Journal of Nutritional Biochemistry* **2012**, *23*, 1600-1608, doi:<https://doi.org/10.1016/j.jnutbio.2011.10.013>.
  41. Brigo, N., Pfeifhofer-Obermair, C., Tymoszuk, P., Demetz, E., Engl, S., Barros-Pinkelnig, M., Dichtl, S., Fischer, C., Valente De Souza, L., Petzer, V.; et al. Cytokine-Mediated Regulation of ARG1 in Macrophages and Its Impact on the Control of Salmonella enterica Serovar Typhimurium Infection. *Cells* **2021**, *10*, doi:10.3390/cells10071823.

**Copyright:** © 2022 The authors. This is an Open Access preprint (not peer-reviewed) distributed under the terms of the Creative Commons Attribution License, which permits unrestricted use, distribution, and reproduction in any medium, provided the original authors and source are credited. © remains with the authors, who have granted MitoFit Preprints an Open Access publication license in perpetuity.



## Supplement

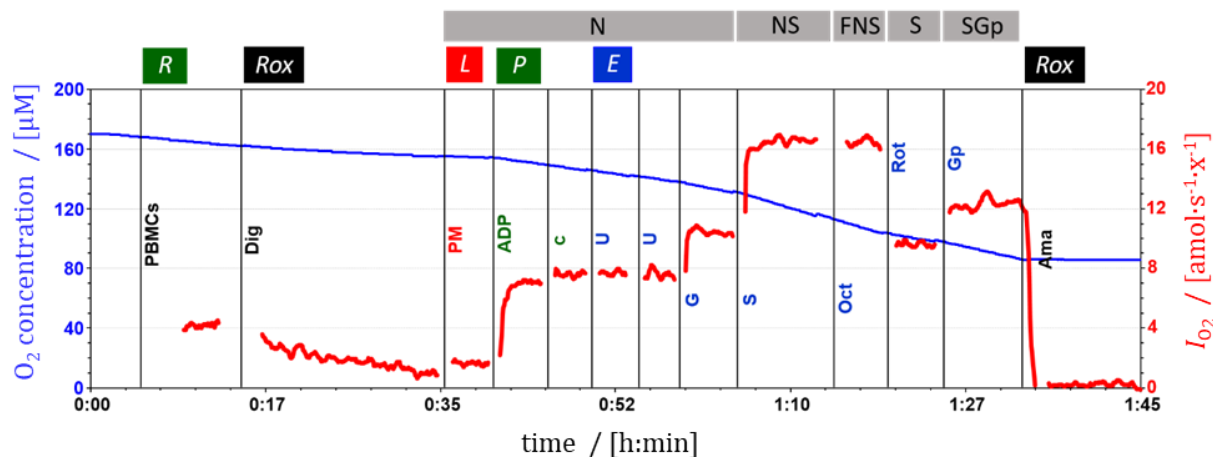


**Figure S1. Representative trace of substrate-uncoupler-inhibitor titration (SUIT, SUIT-001 O2 ce-pce D003 [38]) protocol for measurement of PBMC mitochondrial respiration using high-resolution respirometry.** ROUTINE (*R*) respiration was measured in the presence of isolated PBMCs. Subsequently, the plasma membrane was permeabilized using digitonin (*Dig*): Residual oxygen consumption (*Rox*); pyruvate and malate (*PM*) in the absence of adenosine diphosphate (*ADP*) to measure NADH-linked (*N*) LEAK-respiration (*L*); kinetically saturating concentration of *ADP* to measure OXPHOS-capacity (*P*); cytochrome *c* (*c*) to detect mitochondrial outer membrane integrity; uncoupler titrations (*U*) to measure electron transfer (*ET*) capacity (*E*); glutamate (*G*) to measure N-linked *ET* capacity; succinate (*S*) to measure NS-linked *ET* capacity; octanoylcarnitine (*Oct*) to detect FNS-linked *ET* capacity; Complex I inhibitor rotenone (*Rot*) to measure S-*ET* capacity; glycerol-3-phosphate (*Gp*) to measure SGp-*ET* capacity; antimycin A (*Ama*) to detect *Rox*. Experiment: 2020-07-22 PS3-01 IDA 6 Chamber A. O<sub>2</sub> concentration (blue trace) and O<sub>2</sub> flow per cell (red trace).

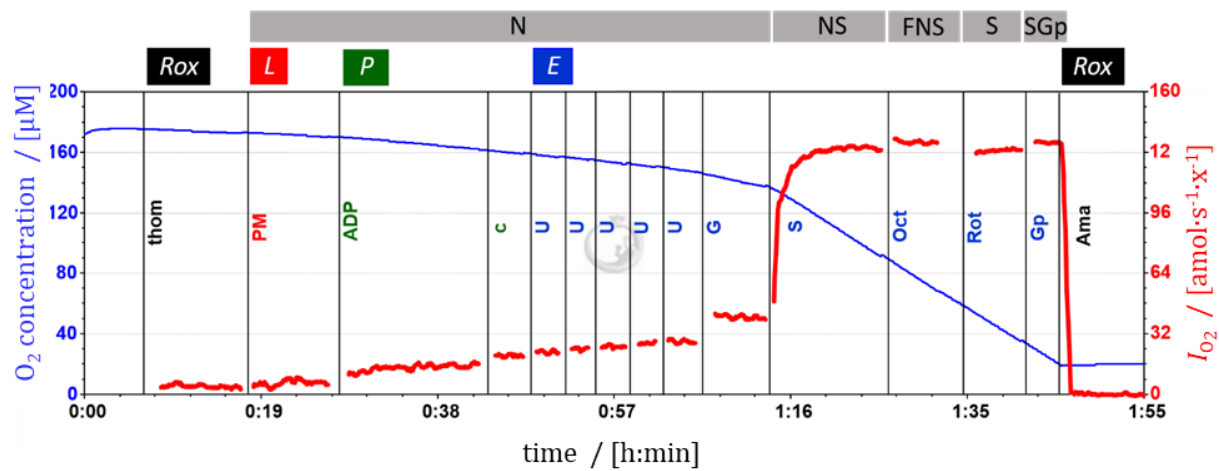


**Figure S2. Representative trace of SUIT protocol (SUIT-001 O2 mt D001 [39]) for measurement of liver mitochondrial respiration using high-resolution respirometry.** *Rox* measured in the presence of liver homogenate (*thom*); pyruvate and malate (*PM*) in the absence of adenosine diphosphate (*ADP*) to measure NADH-linked (*N*) LEAK-respiration (*L*); kinetically saturating concentration of *ADP* to measure OXPHOS-capacity (*P*); cytochrome *c* (*c*) to detect mitochondrial outer membrane integrity; uncoupler titrations (*U*) to measure electron transfer (*ET*) capacity (*E*); glutamate (*G*) to measure N-linked *ET* capacity; succinate (*S*) to measure NS-linked *ET* capacity; octanoylcarnitine (*Oct*) to detect FNS-linked *ET* capacity; Complex I inhibitor rotenone (*Rot*) to measure S-*ET* capacity; glycerol-3-phosphate (*Gp*) to measure SGp-*ET* capacity; antimycin A (*Ama*) to detect *Rox*. Experiment: 2020-07-22 PS3-01 IDA 6 Chamber B. O<sub>2</sub> concentration (blue trace) and O<sub>2</sub> flux per mass (red trace).